

Multipolar Black Body Radiation Shifts for the Single Ion Clocks

¹Bindiya Arora, ²D. K. Nandy and ²B. K. Sahoo *

¹*IISER Mohali, Sector 81 Mohali, P.O. Manouli, 140306, India*

²*Theoretical Physics Division, Physical Research Laboratory, Ahmedabad-380009, India*

(Dated: Received date; Accepted date)

Appraising the projected 10^{-18} fractional uncertainty in the optical frequency standards using singly ionized ions, we estimate the black-body radiation (BBR) shifts due to the magnetic dipole (M1) and electric quadrupole (E2) multipoles of the magnetic and electric fields, respectively. Multipolar scalar polarizabilities are determined for the singly ionized calcium (Ca^+) and strontium (Sr^+) ions using the relativistic coupled-cluster method; though the theory can be exercised for any single ion clock proposal. The expected energy shifts for the respective clock transitions are estimated to be $4.38(3) \times 10^{-4}$ Hz for Ca^+ and $9.50(7) \times 10^{-5}$ Hz for Sr^+ . These shifts are large enough and may be prerequisite for the frequency standards to achieve the foreseen 10^{-18} precision goal.

PACS numbers: 31.25.-v, 32.10.Dk, 06.30.Ft, 32.80.-t

I. INTRODUCTION

Optical transitions with ultranarrow frequencies in the single positively charged ions which use advanced laser cooling and trapping techniques are of current interest for frequency standards [1–3]. Some of the successful single ion optical atomic clocks are Hg^+ [4, 5], Ca^+ [6], Sr^+ [7, 8], Al^+ [3, 9], Yb^+ [10] etc., among these the fractional uncertainty in Hg^+ and Al^+ have already reached 10^{-17} [3]. A new range of experiments are also proposed for other ions like Ba^+ [11, 12], Ra^+ [13], In^+ [14, 15], Yb^+ [16] etc. More precise frequency standards will open-up possibilities to study the underlying physics related to fundamental constants, probing new elementary physics, more importantly it can help in improving the present day global positioning systems and also tracking of deep-space probes [1, 5, 17–19].

One of the major fortifications to attain smaller fractional uncertainties in the optical frequency standard measurements using ions is the accurate measurement of black-body radiation (BBR) shifts. The considered standard frequency is shifted from the atomic resonance value due to the interaction of the ion with the external stray electromagnetic fields present in and around the experimental apparatus [20]. The BBR shift is caused by the isotropic field radiated due to finite temperature of the apparatus [20–22].

The dominant contribution to the BBR-induced energy shift is from the electric dipole (E1) component of the radiation field; which have been gauged by many groups for a number of ions using the relativistic theories [13, 23–28]. However, there is absolutely no rigorous estimate of the BBR shift due to higher multipoles for any proposed scheme. Following derivations for E1 BBR shift in [20–22], Porsev and Derevianko have given a generalized derivation [25] to deduce the BBR shifts spawned by any

multipole component of the electromagnetic field.

Two of the proficiency gadgets for the optical frequency standards are with a single calcium ion ($^{43}\text{Ca}^+$) [29] trapped in a Paul trap and with a strontium ion ($^{88}\text{Sr}^+$) confined in an endcap trap [7, 30]. The considered clock transitions in these ions are the $s_{1/2} \rightarrow d_{5/2}$ transitions operating in the optical regime, the principles are similar to the proposed Ba^+ [11, 12], Ra^+ [13] and Yb^+ [10, 16] based frequency standards. A major advantage of using $^{43}\text{Ca}^+$ ion is that the radiation required for cooling, repumping, and clock transition is easily produced by non-bulky solid state or diode laser [29]. The reported frequency measurements of the transition for frequency standard in $^{88}\text{Sr}^+$ have achieved a spectral resolution of better than 1.5 Hz [7, 30–32]. As has been proclaimed, these experiments have the dexterity to diminish the relative systematic uncertainties to a level of 10^{-17} or below [7, 13]. In such a scenario, it is compelling to estimate the BBR shifts caused by the higher multipoles, especially through the M1 and E2 channels for the experiments comprising the $s_{1/2} \rightarrow d_{5/2}$ transitions as in the above ions. Such an attempt was made by Porsev and Derevianko [25] for divalent atoms like Mg, Ca, Sr, and Yb. In this paper, we extend the work to preview the BBR shifts commenced by the M1 and E2 multipoles in the ions; particularly for the $^{43}\text{Ca}^+$ and $^{88}\text{Sr}^+$ ions where the efficacious experiments are in progress to reduce the uncertainties over their previous measurements [6, 7, 29–32].

The paper is organized as follows: First, we discuss the inception of the BBR shifts which embodies the M1 and E2 contributions of the radiation field. Then, we discuss the method of calculation in the $^{43}\text{Ca}^+$ and $^{88}\text{Sr}^+$ ions subsequently presenting the results for the above multipolar contributions to the BBR shifts in these ions before recapitulating the work. Unless stated otherwise, we use the conventional system of atomic units, a.u., in which e , m_e , $4\pi\epsilon_0$ and the reduced Planck constant \hbar have the numerical value one.

*Email: bijaya@prl.res.in

II. THEORY

The interaction Hamiltonian between an electron in an atomic system with the external propagating electromagnetic field in the Coulomb gauge coupling is given by

$$\begin{aligned} V(r, \omega) &= -c\alpha \cdot \mathbf{A}(r, \omega) \\ &= -c(\alpha \cdot \hat{\epsilon}) \exp(i\mathbf{k} \cdot \mathbf{r}), \end{aligned} \quad (1)$$

where α is the Dirac matrix in operator form, ω is the angular frequency of the field and $\mathbf{k} = k\hat{k}$ and $\hat{\epsilon}$ are its wave vector and polarization direction, respectively. In the presence of this interaction, the energy shift that can occur for an atomic energy level $|\Psi_n\rangle$ with energy $E_n = \omega_n$ can be approximated to [21, 22]

$$\delta E_n(\omega) = \frac{1}{2} \sum_{m \neq n} |V(r, \omega)|^2 \left(\frac{\omega_n - \omega_m}{(\omega_n - \omega_m)^2 - \omega^2} \right). \quad (2)$$

Using the multipolar expansion and in terms of the traditional multipole moments Q_{LM}^λ , we have [33]

$$\begin{aligned} (\alpha \cdot \hat{\epsilon}) \exp(i\mathbf{k} \cdot \mathbf{r}) &= - \sum_{LM} \frac{k^L i^{L+1+\lambda}}{(2L+1)!!} [\mathbf{Y}_{LM}^\lambda(\hat{k}) \cdot \hat{\epsilon}] \\ &\quad \sqrt{\frac{4\pi(2L+1)(L+1)}{L}} Q_{LM}^\lambda, \end{aligned} \quad (3)$$

where $\lambda = 1$ and $\lambda = 0$ represents the electric and magnetic multipoles, respectively.

Using the relations $\mathbf{B} = \nabla \times \mathbf{A}$ and $\mathbf{E} = \frac{i\omega}{c} \mathbf{A}$ and combining all the above expressions, the energy shift for an isotropic field after averaging over ω for all the polarization and propagation directions is given as [22, 25]

$$\begin{aligned} \delta E_n^{(\lambda, L)} &= - \frac{(\alpha T)^{2L+1}}{2J_n + 1} \sum_m |\langle \Psi_n | Q_L^{(\lambda)} | \Psi_m \rangle|^2 \\ &\quad \times F_L \left(\frac{\omega_{mn}}{T} \right), \end{aligned} \quad (4)$$

where J_n is the angular momentum of state $|\Psi_n\rangle$ and

$$\begin{aligned} F_L(y) &= \frac{1}{\pi} \frac{L+1}{L(2L+1)!!(2L-1)!!} \\ &\quad \times \int_0^\infty \left(\frac{1}{y+x} + \frac{1}{y-x} \right) \frac{x^{2L+1}}{e^x - 1} dx. \end{aligned} \quad (5)$$

Here argument $y = \omega_{mn}/T = (\omega_n - \omega_m)/T$. The function $F_L(y)$ is a universal function applicable to all the atoms with argument y depending on the range of the atomic parameters. These functions were first introduced by Farley and Wing [22] in the E1 case and are extended in a general form in this work to emanate simpler forms for the energy shift expressions. In the limit $|y| \gg 1$ which corresponds to the case when the transition energy is much larger than the temperature (T) is of our current interest.

Substituting values from Eq. (A4) in Eq.(4), the BBR shift for $L = 1$ can be expressed as

$$\delta E_n^{(\lambda, 1)} = -\frac{1}{2} \left(\frac{8\pi^3 \alpha^3 (k_B T)^4}{45(2J_n + 1)} \right) \sum_m \frac{|\langle \Psi_n | Q_1^{(\lambda)} | \Psi_m \rangle|^2}{\omega_{mn}}. \quad (6)$$

Now at the room temperature (300 K), the BBR shift for the E1 channel can be given as

$$\begin{aligned} \delta E_n^{E1} &= -\frac{1}{2} \frac{4\pi^3 \alpha^3}{15} (k_B T)^4 \alpha_n^{E1} \\ &= -\frac{1}{2} \langle E_{E1}^2(\omega) \rangle \alpha_n^{E1} \\ &= -\frac{1}{2} (831.9 \text{ V/m})^2 \left[\frac{T(\text{K})}{300} \right]^4 \alpha_n^{E1}, \end{aligned} \quad (7)$$

whereas for the M1 channel can be reduced to

$$\begin{aligned} \delta E_n^{M1} &= -\frac{1}{2} \frac{4\pi^3 \alpha^5}{15} (k_B T)^4 \alpha_n^{M1} \\ &= -\frac{1}{2} \langle B_{M1}^2(\omega) \rangle \alpha_n^{M1} \\ &= -\frac{1}{2} (2.77 \times 10^{-6} \text{ Tesla})^2 \left[\frac{T(\text{K})}{300} \right]^4 \alpha_n^{M1}, \end{aligned} \quad (8)$$

where α_n^{E1} , α_n^{M1} , $\langle E_{E1}^2(\omega) \rangle$ and $\langle B_{M1}^2(\omega) \rangle$ are the scalar E1 polarizability, scalar M1 polarizability, the averaged E1 induced electric field and the averaged M1 induced magnetic fields, respectively.

Similarly, substituting values from Eq. (A5) in Eq. (4), the BBR shifts for $L = 2$ comes out as

$$\delta E_n^{(\lambda, 2)} = -\frac{1}{2} \left(\frac{16(\alpha\pi)^5 (k_B T)^6}{945(2J_n + 1)} \right) \sum_m \frac{|\langle \Psi_n | Q_2^{(\lambda)} | \Psi_m \rangle|^2}{\omega_{mn}}, \quad (9)$$

which corresponds to the E2 and M2 channels.

Therefore, the BBR shift at the room temperature for the E2 channel is given by

$$\begin{aligned} \delta E_n^{E2} &= -\frac{1}{2} \frac{8(\alpha\pi)^5 (k_B T)^6}{189(2J_n + 1)} \alpha_n^{E2} \\ &= -\frac{1}{2} \langle E_{E2}^2(\omega) \rangle \alpha_n^{E2} \\ &= -\frac{1}{2} (7.2 \times 10^{-3} \text{ V/m})^2 \left[\frac{T(\text{K})}{300} \right]^6 \alpha_n^{E2}, \end{aligned} \quad (10)$$

where α_n^{E2} is the scalar E2 polarizability and $\langle E_{E2}^2(\omega) \rangle$ is the averaged E2 induced electric field.

Accumulating all the above expressions, the BBR shifts due to both the M1 and E2 channels for an atomic transition $|\Psi_f\rangle \rightarrow |\Psi_i\rangle$ at room temperature can now be given in the forms

$$\begin{aligned} \delta E_{f \rightarrow i}^{M1} &= -\frac{1}{2} (2.77 \times 10^{-6} \text{ Tesla})^2 \left[\frac{T(\text{K})}{300} \right]^4 \\ &\quad \times (\alpha_f^{M1} - \alpha_i^{M1}), \end{aligned} \quad (11)$$

and

$$\delta E_{f \rightarrow i}^{E2} = -\frac{1}{2}(7.2 \times 10^{-3} \text{V/m})^2 \left[\frac{T(\text{K})}{300} \right]^6 \times (\alpha_f^{E2} - \alpha_i^{E2}), \quad (12)$$

respectively.

III. METHOD OF CALCULATION

In order to determine M1 and E2 polarizabilities in the considered systems, which have closed-shell configurations with one valence electron each, we first calculate the Dirac-Fock (DF) wave function ($|\Phi_0\rangle$) for the corresponding closed-shell configurations, then append the valence orbital (n) to define a new reference state (i.e. $|\Phi_n\rangle = a_n^\dagger |\Phi_0\rangle$) in the Fock space. To obtain the exact atomic wave functions (ASFs), the core, core-valence and valence correlation effects are accounted by defining wave operators Ω_c , Ω_{cn} and Ω_n , respectively. i.e. the exact ASF $|\Psi_n\rangle$ with a valence orbital n is given by

$$|\Psi_n\rangle = a_n^\dagger \Omega_c |\Phi_0\rangle + \Omega_{cn} |\Phi_n\rangle + \Omega_n |\Phi_n\rangle. \quad (13)$$

We adopt the relativistic coupled-cluster (RCC) method in the Fock-space to determine ASFs. With T and S_n representing the core electrons and core electrons with the valence electron excitation operators, respectively, the above ASF in the RCC framework can be encapsulated in a form [12, 13, 26, 27, 34]

$$|\Psi_n\rangle = e^T \{1 + S_n\} |\Phi_n\rangle, \quad (14)$$

where the ASF for the closed-shell configuration is given by Ω_c defining $|\Psi_0\rangle = \Omega_c |\Phi_0\rangle = e^T |\Phi_0\rangle$, $\Omega_{cn} = e^{T(n)} |\Phi_0\rangle$ and $\Omega_n = e^T S_n |\Phi_n\rangle$. We have mentioned $T(n)$ for Ω_{cn} to emphasize on the fact that the T operator in this case excites at least one of the core electrons to the valence orbital. All these correlation effects are coupled in the course of the ASF determination.

The equations determining the coupled-cluster amplitudes and energies are accustomed in compact forms as

$$\langle \Phi_0^* | \{ \widehat{H} e^T \} | \Phi_0 \rangle = \delta_{0,*} \Delta E_{corr} \quad (15)$$

and

$$\begin{aligned} \langle \Phi_n^* | \{ \widehat{H} e^T \} \{ 1 + S_n \} | \Phi_n \rangle &= \langle \Phi_n^* | 1 + S_n | \Phi_n \rangle \\ &\quad \langle \Phi_n | \{ \widehat{H} e^T \} \{ 1 + S_n \} | \Phi_n \rangle \\ &= \langle \Phi_n^* | \delta_{n,*} + S_n | \Phi_n \rangle \Delta E_n, \end{aligned} \quad (16)$$

where the notation $(* = 1, 2)$ represents for the excited hole-particle states, $\widehat{H} e^T$ denotes the connected terms of the Dirac-Coulomb (DC) Hamiltonian (H) with the T operators, ΔE_{corr} and ΔE_v are the correlation energy and attachment energy (also equivalent to negative of the ionization potential (IP)) of the electron of orbital v ,

respectively. It can be noticed that the reference states $|\Phi_0\rangle$ in Eq. (15) and $|\Phi_n\rangle$ in Eq. (16) contain different number of particles, hence the Hamiltonian used in the respective equations describe different number of particles in our Fock space representation. We have considered contributions only from the singly and doubly excited states along with some important valence triple excitations which are included perturbatively; the approach is known as CCSD(T) method in the literature (e.g. see [12, 13, 26, 27, 34]).

To calculate the scalar polarizabilities, it is precedence to adopt an approach similar to [26, 27] or it would be prudent to follow a procedure given in [28]. Such approaches may be required for achieving better accuracies. Accumulating from the previous expressions, the general definition of the scalar polarizability is given by

$$\alpha_n^{Q_\lambda^L} = \frac{1}{\alpha^{2(\lambda-1)}} \frac{2}{(2L+1)} \frac{1}{2J_n+1} \times \sum_m \frac{|\langle \Psi_n | Q_\lambda^L | \Psi_m \rangle|^2}{E_n - E_m}. \quad (17)$$

Procuring the derivations in Eq. (B2), we can now write

$$\alpha_n^{Q_\lambda^L} = \alpha_n^{Q_\lambda^L}(c) + \alpha_n^{Q_\lambda^L}(nc) + \alpha_n^{Q_\lambda^L}(n), \quad (18)$$

where $\alpha_n^{Q_\lambda^L}(c)$, $\alpha_n^{Q_\lambda^L}(nc)$ and $\alpha_n^{Q_\lambda^L}(n)$ are referred to as core, core-valence and valence correlation contributions, respectively.

In the sum-over-states approach as given in Eq. (17), it is convenient to determine the low-lying singly excited states $|\Psi_m\rangle$ with respect to the $|\Psi_n\rangle$ states that are of our interest for both the considered ions. Contributions from these states corresponds to the above mentioned valence correlation contributions, which are the dominant ones compared to the contributions to the part arising from higher level excited states that can be estimated from a lower order perturbation theory. Contrasting to this contribution, it is not possible to estimate the core and core-valence correlation contributions in a similar procedure. As it was stated above, methods describing in [26–28] would be befitting to account them rigorously. Notwithstanding this fact, it will not alter the BBR shifts what is the primary intent of the work. This is because of two reasons: First, the core correlation effect may be notable but in the BBR shift estimation this contribution cancels out between the transition states. However, we calculate them using the third order relativistic many-body perturbation theory (MBPT(3)) to present the total polarizability results. Secondly, it is observed in the earlier works that the core-valence contributions are minuscule in the dipole polarizability determinations [23, 24, 26, 27] which is further verified below in the present work. So it is not necessary to employ a powerful method at the cost of heavy computation to determine these tiny contributions for which we use again the MBPT(3) method

to estimate these contributions within the required precision level. In this approach, we rewrite Eq. (17) as

$$\alpha_n^{Q_\lambda^L} = \frac{1}{\alpha^{2(\lambda-1)}} \frac{2}{(2L+1)} \frac{1}{2J_n+1} \langle \Psi_n | Q_\lambda^L | \Psi_n^{(1)} \rangle \quad (19)$$

where $|\Psi_n^{(1)}\rangle$ is the first order perturbed wave function for $|\Psi_n\rangle$ due to Q_λ^L which is obtained by solving the following equation

$$(H - E_n) |\Psi_n^{(1)}\rangle = (E_n^{(1)} - Q_\lambda^L) |\Psi_n\rangle, \quad (20)$$

where $E_n^{(1)}$ is the energy correction due to Q_λ^L . Some of the important diagrams representing this equation for the core and core-valence correlation effects evaluation are shown in Fig. 1.

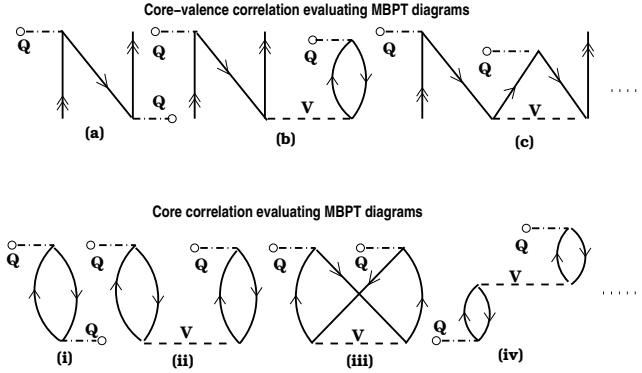


FIG. 1: Few important many-body perturbation theory (MBPT) diagrams used for the core-valence and core correlations estimation.

The reduced transition matrix element of a physical operator Q_λ^L between $|\Psi_f\rangle$ and $|\Psi_i\rangle$ in our approach is calculated using the expression

$$\frac{\langle \Psi_f | Q_\lambda^L | \Psi_i \rangle}{\sqrt{\langle \Psi_f | \Psi_f \rangle \langle \Psi_i | \Psi_i \rangle}} = \frac{\langle \Phi_f | \{1 + S_f^\dagger\} \overline{Q_\lambda^L} \{1 + S_i\} | \Phi_i \rangle}{\sqrt{\mathcal{N}_f \mathcal{N}_i}}, \quad (21)$$

where $\overline{Q_\lambda^L} = e^{T^\dagger} Q_\lambda^L e^T$ and $\mathcal{N}_n = \langle \Phi_n | e^{T^\dagger} e^T + S_n^\dagger e^{T^\dagger} e^T S_n | \Phi_n \rangle$ involve two non-truncating series in the above expression. We have mentioned concisely the procedure for calculating these expressions in the appendix in [34]. We evaluate them keeping terms up to fourth order in Coulomb interaction.

The single particle orbital reduced matrix elements for the corresponding M1 and E2 cases are taken as

$$\langle \kappa_f || m1 || \kappa_i \rangle = \frac{(\kappa_f + \kappa_i)}{\alpha} \langle -\kappa_f || C^{(1)} || \kappa_i \rangle \int_0^\infty dr r (P_f(r) Q_i(r) + Q_f(r) P_i(r)), \quad (22)$$

and

$$\langle \kappa_f || e2 || \kappa_i \rangle = \langle \kappa_f || C^{(2)} || \kappa_i \rangle \int_0^\infty dr r^2 (P_f(r) P_i(r) + Q_f(r) Q_i(r)), \quad (23)$$

where $P(r)$ and $Q(r)$ represent the radial parts of the large and small components of the single particle Dirac orbitals, respectively. The reduced Racah coefficients are given by

$$\langle \kappa_f || C^{(k)} || \kappa_i \rangle = (-1)^{j_f+1/2} \sqrt{(2j_f+1)(2j_i+1)} \begin{pmatrix} j_f & k & j_i \\ 1/2 & 0 & -1/2 \end{pmatrix} \pi(l_{\kappa_f}, k, l_{\kappa_i}), \quad (24)$$

with

$$\pi(l, m, l') = \begin{cases} 1 & \text{for } l + m + l' = \text{even} \\ 0 & \text{otherwise.} \end{cases} \quad (25)$$

We have used Gaussian type orbitals (GTOs) to construct the single particle orbitals for the Dirac-Fock ($|\Phi_0\rangle$) wave function calculation. The large and small components of the Dirac orbitals in this case are expressed as

$$P_\kappa(r) = \sum_k c_k^P r^{l_\kappa} e^{-\alpha_\kappa r^2} \quad (26)$$

and

$$Q_\kappa(r) = \sum_k c_k^Q r^{l_\kappa} \left(\frac{d}{dr} + \frac{\kappa}{r} \right) e^{-\alpha_\kappa r^2}, \quad (27)$$

where the summation over k is for the total number of GTOs used in each symmetry, c_k^P and c_k^Q are the normalization constants for the large and small components, respectively, and we use $(\frac{d}{dr} + \frac{\kappa}{r})$ operator to expand the small component Dirac orbitals to maintain the kinetic balance condition with its large component. In the present calculations, we have considered 9 relativistic symmetries (up to g symmetry) and 28 GTOs for each symmetry to generate the orbitals. In order to optimise the exponents to describe orbitals from various symmetries in a smooth manner, we use the even tempering condition

$$\alpha_k = \alpha_0 \beta^{k-1}, \quad (28)$$

where α_0 and β are two arbitrary parameters that are chosen suitably for different symmetries.

We have considered $\alpha_0 = 7.5 \times 10^{-4}$ for all the symmetries and β s are optimised to be 2.56, 2.58, 2.61, 2.75 and 2.83 for s , p , d , f and g orbitals, respectively. For the RCC calculations, we have considered excitations up to first 16s, 16p, 16d, 14f and 13g orbitals while contributions from other virtual orbitals having large energies are neglected.

TABLE I: Contributions to the $4s_{1/2}$ and $3d_{5/2}$ scalar (α^{M1}) static polarizabilities in $^{43}\text{Ca}^+$ and their uncertainties in units of a_0^3 . The values of the corresponding M1 matrix elements for αQ_0^1 are given in ea_0 .

Transition	Amplitude	α^{M1}
α_n		
$4s_{1/2} \rightarrow$	$5s_{1/2}$	$0.0018(3)$
	$6s_{1/2}$	$0.0013(2)$
	$3d_{3/2}$	$0.0008(1)$
	$4d_{3/2}$	$0.0003(1)$
	$5d_{3/2}$	$0.0001(1)$
	$6d_{3/2}$	$0.0003(1)$
α_c		
α_{cn}		
α_{tail}		
α_{total}		
α_n		
$3d_{5/2} \rightarrow$	$3d_{3/2}$	$1.543(5)$
	$4d_{3/2}$	$0.004(1)$
	$5d_{3/2}$	$0.004(1)$
	$6d_{3/2}$	$0.003(1)$
	$4d_{5/2}$	$0.004(1)$
	$5d_{5/2}$	$0.009(2)$
	$6d_{5/2}$	$0.002(1)$
	$5g_{7/2}$	3.2×10^{-7}
	$6g_{7/2}$	4.6×10^{-7}
α_c		
α_{cn}		
α_{tail}		
α_{total}		

IV. RESULTS AND DISCUSSIONS

As has been emphasized before, precise estimation of the BBR shifts due to M1 and E2 transitions in Ca^+ and Sr^+ are the focus of this work. The uncertainties in these estimations are of two folds: First, the errors associated with the considered excitation energies (EEs). Second, inaccuracies from the estimated transition matrix elements. To abate the uncertainties in the evaluation of the BBR shift for the atomic clock application, we use the experimental EEs from the NIST database [35] for the important singly excited states. Matrix elements for these states are mentioned explicitly along with their uncertainties and respective contributions to the the scalar polarizabilities in Tables I, II, III, and IV. Contributions from the doubly excited states constructed within the configuration space spanned by the considered orbitals for our RCC calculations and from the higher singly excited states which are not mentioned specifically are accounted as α_{tail} using the MBPT(3) method. As shown in Tables I, II, III, and IV, these contributions are rather diminutive to be concerned about. The uncertainties in these results and for the transition matrix elements are estimated taking into account the neglected

TABLE II: Contributions to the $5s_{1/2}$ and $4d_{5/2}$ scalar (α^{M1}) static polarizabilities in $^{88}\text{Sr}^+$ and their uncertainties in units of a_0^3 . The values of the corresponding M1 matrix elements for αQ_0^1 are given in ea_0 .

Transition	Amplitude	α^{M1}
α_n		
$5s_{1/2} \rightarrow$	$6s_{1/2}$	$1.35(2) \times 10^{-3}$
	$7s_{1/2}$	$1.24(1) \times 10^{-3}$
	$8s_{1/2}$	$1.00(1) \times 10^{-3}$
	$9s_{1/2}$	$1.00(1) \times 10^{-3}$
	$4d_{3/2}$	$5.0(3) \times 10^{-5}$
	$5d_{3/2}$	$1.0(1) \times 10^{-5}$
	$6d_{3/2}$	$1.0(1) \times 10^{-6}$
	$7d_{3/2}$	$3.0(2) \times 10^{-6}$
α_c		
α_{cn}		
α_{tail}		
α_{total}		
α_n		
$4d_{5/2} \rightarrow$	$4d_{3/2}$	$1.545(6)$
	$5d_{3/2}$	$0.009(2)$
	$6d_{3/2}$	$0.006(1)$
	$7d_{3/2}$	$0.004(1)$
	$5d_{5/2}$	$0.003(1)$
	$6d_{5/2}$	$0.003(1)$
	$7d_{5/2}$	$0.002(1)$
	$5g_{7/2}$	$3.2(5) \times 10^{-7}$
	$6g_{7/2}$	$3.0(4) \times 10^{-7}$
α_c		
α_{cn}		
α_{tail}		
α_{total}		

contributions and numerical calculations.

We first present the static scalar α^{M1} polarizabilities in the Ca^+ and Sr^+ ions in Table I and Table II, respectively, for both the ground and $d_{5/2}$ states. As seen in these tables, α^{M1} s are very small for the corresponding ground states in both the ions, however they are reported in this paper for the completeness of the results. Contributions from the core correlations are the largest in determining these results and they will be cancelled while estimating the BBR shifts due to M1 multipole. Therefore, the ground state M1 polarizability contributions in the considered ions can be neglected. Essentially, the contributions to the α^{M1} polarizabilities in the $d_{5/2}$ states are overwhelmingly dominant owing to the very small energy gap of their fine structure partner states and contributions from all other states are small. The M1 matrix elements between the $d_{3/2} - d_{5/2}$ transitions in the considered ions were also reported earlier by us [36] and they seem to be very consistent. From our calculations, we obtain α^{M1} for the $3d_{5/2}$ and $4d_{5/2}$ states as $-957(6)$ a.u. and $-208(2)$ a.u. in the Ca^+ and Sr^+ ions, respectively. The uncertainty in the final result is

TABLE III: Contributions to the $4s_{1/2}$ and $3d_{5/2}$ scalar (α^{E2}) static polarizabilities in $^{43}\text{Ca}^+$ and their uncertainties in units of a_0^5 . The values of the corresponding E2 matrix elements for Q_1^2 are given in ea_0^2 .

Transition		Amplitude	α^{E2}
α_n			
$4s_{1/2} \rightarrow$	$3d_{3/2}$	8.12(5)	212(3)
	$4d_{3/2}$	12.51(8)	121(2)
	$5d_{3/2}$	3.89(4)	9.1(2)
	$6d_{3/2}$	5.44(6)	16.2(4)
	$3d_{5/2}$	9.97(6)	318(3)
	$4d_{5/2}$	15.30(9)	181(2)
	$5d_{5/2}$	4.75(5)	13.6(3)
	$6d_{5/2}$	6.67(6)	24.2(4)
α_c			6.15(8)
α_{cn}			0.0
α_{tail}			5.36(5)
α_{total}			906(5)
Other works			712.91 ^a , 871 ^b
α_n			
$3d_{5/2} \rightarrow$	$4s_{1/2}$	9.97(6)	-106(1)
	$5s_{1/2}$	4.99(5)	9.4(2)
	$6s_{1/2}$	1.22(2)	0.38(1)
	$3d_{3/2}$	3.90(4)	-3657(75)
	$4d_{3/2}$	4.32(5)	6.3(1)
	$5d_{3/2}$	1.38(2)	0.47(1)
	$6d_{3/2}$	1.08(1)	0.25(5)
	$4d_{5/2}$	8.63(5)	25.2(3)
	$5d_{5/2}$	2.75(3)	1.87(4)
	$6d_{5/2}$	2.16(2)	1.02(2)
	$5g_{7/2}$	1.58(2)	0.56(1)
	$6g_{7/2}$	1.04(1)	0.210(4)
	$5g_{9/2}$	5.57(5)	7.0(1)
	$6g_{9/2}$	3.67(4)	2.62(6)
α_c			6.15(8)
α_{cn}			0.18(2)
α_{tail}			-4.29(7)
α_{total}			-3706(75)
References: ^a [37]			
^b [38]			

obtained by adding the uncertainty from each contribution in quadrature. As shown in Table II the uncertainty in the $d_{5/2}$ state polarizability value is dominated by the uncertainty in the $d_{3/2} - d_{5/2}$ contribution.

We now turn to the α^{E2} results. Our calculated results for the ground and $3d_{5/2}$ states in Ca^+ are given in Table III. Both the results are comparatively large with opposite signs. The largest contribution to the ground state polarizability comes from the $3d$ states followed by the $4d$ states. The core contribution is comparatively small and the tail contribution to the ground state polarizability is zero due to the absence of occupied d states in Ca^+ . There are two more calculations available in the literature on the same using the RCC methods with different level of approximations [37, 38]. Result reported in

[37] is *ab initio* and are obtained from a linear response theory based calculation. Linear approximation in the RCC method is being considered to evaluate the corresponding transition matrix elements for the estimation of the ground state polarizability in [38] using a sum-over-states approach like the present work. All the results are of same order in magnitude. The *ab initio* result seems to be little lower than the results obtained from the sum-over-states approach due to the additional uncertainties from the calculated energies that justifies for considering the experimental energies in these calculations. However, it can be noticed that the differences in these results will not alter the BBR shift results which can be apparent from the following finding on the E2 polarizability contributions. To our knowledge, no other quadrupole polarizability result is available for the $3d_{5/2}$ state in Ca^+ to compare with ours. Again, contribution from its fine structure partner is the decisive factor for the final result followed by a significant contribution from the ground state. In Table IV, we present α^{E2} results for the ground and $4d_{5/2}$ states in Sr^+ . The magnitudes of the ground state result in this ion is larger than Ca^+ , while for the corresponding $d_{5/2}$ it is other way around. There are no results available to the best of our knowledge to compare our results with them. The trend of the contributions from different transitions is almost similar for corresponding states in both the ions. We add the uncertainty from each contribution in quadrature to obtain the final uncertainty in E2 polarizability values.

Using the above values of the polarizabilities, we obtain the BBR shift due to the M1 multipole for the $4s\ ^2S_{1/2} \rightarrow 3d\ ^2D_{5/2}$ transition in Ca^+ at the room temperature (300 K) to be $4.38(3) \times 10^{-4}$ Hz. Similarly, this result comes out to be $9.50(7) \times 10^{-5}$ Hz for the $5s\ ^2S_{1/2} \rightarrow 4d\ ^2D_{5/2}$ transition in Sr^+ . Contributions from the E2 multipole are very small and below the uncertainties of the above results and hence can be neglected for the present purpose of the work. However, the reported quadrupole polarizabilities for all the considered states may be useful elsewhere. It has to be noticed that the BBR shifts due to the E1 multipole are 0.38(1) Hz [27, 38] and 0.22(1) Hz [26] for the corresponding transitions in Ca^+ and Sr^+ , respectively.

V. CONCLUSION

In summary, we have estimated the black-body radiation shifts due to the magnetic dipole and electric quadrupole multipoles for the $4s\ ^2S_{1/2} \rightarrow 3d\ ^2D_{5/2}$ and $5s\ ^2S_{1/2} \rightarrow 4d\ ^2D_{5/2}$ transitions in the singly ionized calcium and strontium, respectively. The contribution due to the former is the decisive in this case. Nevertheless, the reported polarizabilities for the considered states which are rarely studied in the above ions may also be useful for other purposes. It may be imperative to contemplate the reported shifts which are given as $4.38(3) \times 10^{-4}$ Hz and $9.50(7) \times 10^{-5}$ Hz in the considered ions to achieve

TABLE IV: Contributions to the $5s_{1/2}$ and $4d_{5/2}$ scalar (α_0^{E2}) static polarizabilities in $^{88}\text{Sr}^+$ and their uncertainties in units of a_0^5 . The values of the corresponding E2 matrix elements for Q_1^2 are given in ea_0^2 .

Transition	Amplitude	α^{E2}
α_n		
$5s_{1/2} \rightarrow 4d_{3/2}$	11.25(7)	382(5)
$5s_{1/2} \rightarrow 5d_{3/2}$	12.87(8)	136(2)
$5s_{1/2} \rightarrow 6d_{3/2}$	5.00(5)	16.2(3)
$5s_{1/2} \rightarrow 7d_{3/2}$	3.11(4)	5.7(1)
$5s_{1/2} \rightarrow 4d_{5/2}$	13.91(8)	572(6)
$5s_{1/2} \rightarrow 5d_{5/2}$	15.64(9)	201(2)
$5s_{1/2} \rightarrow 6d_{5/2}$	5.97(6)	23.3(4)
$5s_{1/2} \rightarrow 7d_{5/2}$	3.76(4)	8.3(1)
α_c		14.50(9)
α_{cn}		$-1.7(2) \times 10^{-8}$
α_{tail}		6.35(8)
α_{total}		1366(9)
α_n		
$4d_{5/2} \rightarrow 5s_{1/2}$	13.91(8)	-191(2)
$4d_{5/2} \rightarrow 6s_{1/2}$	1.31(1)	0.77(1)
$4d_{5/2} \rightarrow 7s_{1/2}$	1.90(2)	1.05(2)
$4d_{5/2} \rightarrow 8s_{1/2}$	0.96(1)	0.231(5)
$4d_{5/2} \rightarrow 9s_{1/2}$	0.72(1)	0.119(4)
$4d_{5/2} \rightarrow 4d_{3/2}$	6.08(6)	-1930(38)
$4d_{5/2} \rightarrow 5d_{3/2}$	5.63(6)	12.1(3)
$4d_{5/2} \rightarrow 6d_{3/2}$	1.83(2)	0.92(2)
$4d_{5/2} \rightarrow 7d_{3/2}$	1.14(1)	0.315(6)
$4d_{5/2} \rightarrow 5d_{5/2}$	11.17(7)	47.4(6)
$4d_{5/2} \rightarrow 6d_{5/2}$	3.65(5)	3.7(1)
$4d_{5/2} \rightarrow 7d_{5/2}$	2.28(3)	1.27(3)
$4d_{5/2} \rightarrow 5g_{7/2}$	2.73(3)	1.76(4)
$4d_{5/2} \rightarrow 6g_{7/2}$	2.21(2)	1.11(2)
$4d_{5/2} \rightarrow 5g_{9/2}$	9.64(7)	22.0(3)
$4d_{5/2} \rightarrow 6g_{9/2}$	7.80(6)	13.7(2)
α_c		14.50(9)
α_{cn}		0.24(3)
α_{tail}		-4.83(5)
α_{total}		-2005(38)

the 10^{-18} precision uncertainty in the proposed clock experiments.

Acknowledgement

The work of B.A. was supported by the Department of Science and Technology, India. Computations were carried out using 3TFLOP HPC Cluster at Physical Research Laboratory, Ahmedabad.

Appendix A: Farley & Wing's functions

With the aid $|y| \gg 1$, the following the expression

$$F_L(y) = \frac{1}{\pi} \frac{L+1}{L(2L+1)!!(2L-1)!!} \times \int_0^\infty \left(\frac{1}{y+x} + \frac{1}{y-x} \right) \frac{x^{2L+1}}{e^x - 1} dx, \quad (\text{A1})$$

gives for $L = 1$ as

$$\begin{aligned} F_1(y) &= \frac{2}{3\pi} \int_0^\infty \left(\frac{1}{y+x} + \frac{1}{y-x} \right) \frac{x^3}{e^x - 1} dx \\ &= \frac{2}{3\pi} \left(\frac{2}{y} \int_0^\infty \frac{x^3}{e^x - 1} dx + \frac{2}{y^3} \int_0^\infty \frac{x^5}{e^x - 1} dx \right). \end{aligned} \quad (\text{A2})$$

Further by using the definite integral value

$$\int_0^\infty \frac{x^{2n-1}}{e^{px} - 1} dx = (-1)^{n-1} \left(\frac{2\pi}{p} \right)^{2n} \frac{B_{2n}}{4n}, \quad (\text{A3})$$

where B_{2n} is the Bernoulli number, $F_1(y)$ reduces to

$$F_1(y) = \frac{4\pi^4}{45y}. \quad (\text{A4})$$

Similarly for $L = 2$, the above expression turns out to be

$$\begin{aligned} F_2(y) &= \frac{1}{30\pi} \int_0^\infty \left(\frac{1}{y+x} + \frac{1}{y-x} \right) \frac{x^5}{e^x - 1} dx \\ &= \frac{1}{15y} \int_0^\infty \frac{x^5}{e^x - 1} dx + \frac{2}{y^3} \int_0^\infty \frac{x^7}{e^x - 1} dx \\ &= \frac{8\pi^5}{945y}. \end{aligned} \quad (\text{A5})$$

Appendix B: Square of the matrix element

In our approach, we write

$$|\Psi_n\rangle = a_n^\dagger \Omega_c |\Phi_0\rangle + \Omega_{cn} |\Phi_v\rangle + \Omega_n |\Phi_v\rangle. \quad (\text{B1})$$

With this expression, the square of the matrix element of any arbitrary operator O can be expressed as

$$\begin{aligned} \langle \Psi_n | O | \Psi_m \rangle^2 &= \langle \Psi_n | O | \Psi_m \rangle \langle \Psi_m | O | \Psi_n \rangle \\ &= \langle \Phi_0 | \Omega_c^\dagger O \Omega_m \Omega_m^\dagger O \Omega_c | \Phi_0 \rangle \\ &\quad + \langle \Phi_0 | \Omega_c^\dagger O \Omega_{cm} \Omega_{cm}^\dagger O \Omega_c | \Phi_0 \rangle \\ &\quad + \langle \Phi_n | \Omega_{cn}^\dagger O \Omega_c \Omega_c^\dagger O \Omega_{cn} | \Phi_n \rangle \\ &\quad + \langle \Phi_n | \Omega_n^\dagger O \Omega_c \Omega_c^\dagger O \Omega_n | \Phi_n \rangle \\ &\quad + \langle \Phi_n | \Omega_n^\dagger O \Omega_{cm} \Omega_{cm}^\dagger O \Omega_n | \Phi_n \rangle \\ &\quad + \langle \Phi_n | \Omega_n^\dagger O \Omega_m \Omega_m^\dagger O \Omega_n | \Phi_n \rangle, \end{aligned} \quad (\text{B2})$$

where we have facilitated the generalized Wick's theorem to derive these terms and assumed all the operators are in normal order form and only the connected terms are survived. For simplicity the first two terms, the second term and the last three terms are categorized into core (c), core-valence (cn) and valence (n) contributions,

respectively; i.e. in an abbreviate form it is given as

$$\begin{aligned} \langle \Psi_n | O | \Psi_m \rangle^2 = & \langle \Psi_n | O | \Psi_m \rangle_c^2 + \langle \Psi_n | O | \Psi_m \rangle_{cn}^2 \\ & + \langle \Psi_n | O | \Psi_m \rangle_n^2. \end{aligned} \quad (\text{B3})$$

-
- [1] P. Gill, *Metrologia* **42**, S125 (2005).
[2] S. A. Diddams *et al.*, *Science* **293** 825 (2001).
[3] T. Rosenband *et al.*, *Science* **319**, 1808 (2008).
[4] W. H. Oskay, S. A. Diddams, E. A. Donley, T. M. Fortier, T. P. Heavner, L. Hollberg, W. M. Itano, S. R. Jefferts, M. J. Delaney, K. Kim, F. Levi, T. E. Parker and J. C. Bergquist, *Phys. Rev. Lett.* **97**, 020801 (2006).
[5] S. Bize *et al.*, *Phys. Rev. Lett.* **90**, 150802 (2003).
[6] K. Matsubara, K. Hayasaka, Y. Ling, H. Ito, S. Nagano, M. Kajita, and M. Hosokawa, *Appl. Phys. Express* **1**, 067011 (2008).
[7] H. S. Margolis, G. P. Barwood, G. Huang, H. A. Klein, S. N. Lea, K. Szymaniec and P. Gill, *Science* **306** 19 (2004).
[8] P. Dube, A. A. Madej, J. E. Bernard, L. Marmet, J. S. Boulanger and S. Cundy, *Phys. Rev. Lett.* **95**, 033001 (2005).
[9] C. W. Chou, D. B. Hume, J. C. J. Koelemeij, D. J. Wineland and T. Rosenband, *Phys. Rev. Lett.* **104**, 070802 (2010).
[10] T. Schneider, E. Peik and Chr. Tamm, *Phys. Rev. Lett.* **94**, 230801 (2005).
[11] J. A. Sherman, W. Trimble, S. Metz, W. Nagourney and N. Fortson, e-print physics/0504013.
[12] B. K. Sahoo, *Phys. Rev. A* **74**, 020501(R) (2006).
[13] B. K. Sahoo, B. P. Das, R. K. Chaudhuri, D. Mukherjee, R. G. E. Timmermans and K. Jungmann, *Phys. rev. A* **76**, 040504(R) (2007).
[14] Th. Becker, J. v. Zanthier, A. Yu. Nevsky, Ch. Schwedes, M. N. Skvortsov, H. Walther and E. Peik, *Phys. Rev. A* **63**, 051802(R) (2001).
[15] Y. H. Wang, R. Dumke, T. Liu, A. Stejskal, Y. N. Zhao, J. Zhang, Z. H. Lu, L. J. Wang, T. Becker and H. Walther, *Opt. Commun.* **273**, 526 (2007).
[16] K. Hosaka, S. A. Webster, A. Stannard, B. R. Walton, H. S. Margolis and P. Gill, *Phys. Rev. A* **79**, 033403 (2009).
[17] C. W. Chou, D. B. Hume, T. Rosenband and D. J. Wineland, *Science* **329**, 1630 (2010).
[18] V. A. Dzuba and V. V. Flambaum, *Phys. Rev. A* **61**, 034502 (2000).
[19] V. V. Flambaum and A. F. Tedesco, *Phys. Rev. C* **73**, 055501 (2006).
[20] M. Mizushima, *Phys. Rev.* **133**, A414 (1964).
[21] S. H. Autler and C. H. Townes, *Phys. rev.* **100**, 703 (1955).
[22] J. W. Farley and W. H. Wing, *Phys. Rev. A* **23**, 2397 (1981).
[23] Bindiya Arora, M. S. Safronova and Charles W. Clark, *Phys. Rev. A*, **76**, 052516 (2007).
[24] Dansha Jiang, Bindiya Arora, M. S. Safronova and Charles W. Clark, *J. Phys. B: At. Mol. Opt. Phys.*, **42**, 154020 (2009).
[25] S. G. Porsev and A. Derevianko, *Phys. Rev. A*, **74**, 020502(R) (2006).
[26] B. K. Sahoo, R. G. E. Timmermans, B. P. Das and D. Mukherjee, *Phys. Rev. A* **80**, 062506 (2009).
[27] B. K. Sahoo, B. P. Das and D. Mukherjee, *Phys. Rev. A* **79**, 052511 (2009).
[28] M. Kallay, H. S. Nataraj, B. K. Sahoo, B. P. Das and L. Visscher, *Phys. Rev. A* **83**, 030503 (2011).
[29] C. Champenois, M. Houssin, C. Lisowski, M. Knoop, G. Hagel, M. Vedel and F. Vedel, *Phys. Lett. A*, **331**, 298 (2004).
[30] A. A. Madej, J. E. Bernard, P. Dube and L. Marmet, *Phys. Rev. A*, **70**, 012507 (2004).
[31] H. S. Margolis, G. Huang, G.P. barwood, S. N. Lea, H. A. Klein, W. R. C. Rowley and P. Gill, *Phys. Rev. A*, **67**, 032501 (2003).
[32] J. E. Bernard, A. A. Madej, L. Marmet, B. G. Whitford, K. J. Siemsen and S. Cundy, *Phys. Rev. Lett.*, **82**, 3228 (1999).
[33] W. R. Johnson, D. R. Plante and J. Sapirstein, *Adv. At. Mol. Opt. Phys.* **35**, 255 (1995).
[34] D. Mukherjee, B. K. Sahoo, H. S. Nataraj and B. P. Das, *J. Phys. Chem. A* **113**, 12549 (2009) and *references therein*.
[35] Yu. Ralchenko, F. -C. Jou, D. E. Kelleher, A. E. Kramida, A. Musgrove, J. Reader, W. L. Wiese and K. Olsen., NIST Atomic Spectra Database, note = (version 3.1.2). [Online]. Available: <http://physics.nist.gov/asd3> [2007, August 29]. National Institute of Standards and Technology, Gaithersburg, MD,(2005).
[36] B. K. Sahoo, Md. R. Islam, B. P. Das, R. K. Chaudhuri and D. Mukherjee, *Phys. Rev. A* **74**, 062504 (2006).
[37] B. K. Sahoo, *Chem. Phys. Lett.* **448**, 144 (2007).
[38] M. S. Safronova and U. I. Safronova, *Phys. Rev. A* **83**, 012503 (2011).